RSC Advances

PAPER

View Article Online
View Journal | View Issue

Cite this: *RSC Adv.*, 2020, **10**, 2075

Metallic Ti_3O_5 hierarchical porous microspheres with an enhanced photothermal property†

Ruifeng Du,[ab] Wei Liu,[b] Hua Bai,[b] Hongtao Wang*[a] and Guangcheng Xi*[b]

Received 5th November 2019
Accepted 16th December 2019

DOI: 10.1039/c9ra09147e

rsc.li/rsc-advances

γ-Ti_3O_5 is one kind of prominent non-stoichiometric metal oxide due to its intriguing ability in electric and electrochemical behaviors. This work reports another attractive property of γ-Ti_3O_5 hierarchical porous microspheres, the extremely effective photothermal property with a high photothermal conversion efficiency. Theory and experimental results indicate that γ-Ti_3O_5 hierarchical porous microspheres possess metallic features and display very strong localized surface plasma resonance effects over the visible and near-infrared region. Under simulated sunlight or near infrared light, the metallic γ-Ti_3O_5 exhibits a photothermal conversion efficiency of up to 65.29%. Under irradiation by a near-infrared laser with a wavelength of 808 nm, the γ-Ti_3O_5 hierarchical porous microspheres can significantly inhibit cancer cell viability *in vitro* and disrupt tumor tissue growth *in vivo* in a short period. *In vitro* and *in vivo* toxicity experiments demonstrate that it has good biocompatibility. The ultrahigh photothermal conversion efficiency and biocompatibility make the γ-Ti_3O_5 very attractive for technological uses in photothermal therapy, solar energy utilization, and infrared light detection and so on.

1. Introduction

Titanium oxides are one type of the most popular compounds among metal oxides due to their outstanding photocatalytic activity, photoelectric conversion efficiency and electrochemical activity and so on.[1,2] Ti_3O_5 is an attractive titanium oxide with distinct physical properties. It is non-stoichiometric and crystallizes in several structural forms. γ-Ti_3O_5 is a unique metallic phase of Ti_3O_5 with high-performance and photoinduced phase-transition.[3] It offers interesting prospects for the development of high density optical memory devices.[4] However, there are few reports noting the photothermal properties of metallic γ-Ti_3O_5.

Materials with photothermal properties have great potentials in applications for optical storage, thermo-photovoltaics, photothermal cancer therapy and so on.[5] Photothermal therapy (PTT) is one of cancer therapies with high efficiency and minimal invasiveness.[6,7] It employs near-infrared (NIR) photoabsorbing agents to transfer heat from light, leading to thermal ablation of cancer cells or tumor tissues. The agents should be able to efficiently transfer the absorbed NIR light energy into heat. Various nanomaterials with strong NIR light harvesting ability were reported to be promising in photothermal transferring treatment of cancer, such as (1) noble metal-based nanostructures, including gold nanoparticles,[8–11] nanorods,[12,13] nanoshells,[14] nanocages,[15,16] and Pd nanomaterials;[17,18] (2) carbon-based nanostructures such as carbon nanotubes,[19,20] nanohorns,[21] and graphenes;[22] (3) organic dye compound, including melanin,[23] indocyanine green (ICG),[24] nanoscale coordination polymers[25] and polypyrrole;[26] (4) oxygen vacancy-rich transition metal compounds,[27] including $W_{18}O_{49}$,[28,29] MoO_{3-x},[30] $MoSe_2$ (ref. 31) and Cu_3BiS_3 (ref. 32) *et al.* Among these PTT agents, oxygen vacancy-rich transition metal oxides are considerable appealing owing to their metallic features, strong localized surface plasmon resonance (LSPR) effect, low cost and easy synthesis.[33]

Furthermore, the application of titanium oxides nanoparticles in cosmetics as ultraviolet absorbents has been proved to be effective and biocompatible. Recently, some research reported that the titanium oxides nanoparticles could be used as photodynamic therapy (PDT) agent by utilizing its strong UV absorption.[34–36] However, the cancer therapeutics of titanium oxides is not adequately explored, particularly NIR induced PTT of titanium oxides has not been reported so far.

Herein, this work find that the metallic titanium oxide, γ-Ti_3O_5 hierarchical porous microspheres (HPMs), exhibit effective photothermal property under both simulated sunlight and near infrared light. Their NIR photothermal conversion efficiency has reached fairly high level up to 65.29%. *In vitro* and *in vivo* experiments demonstrated that the metallic γ-Ti_3O_5 HPMs can significantly inhibit cancer cell viability and destruct tumor tissue growth, indicating it is an effective PTT agent for cancer therapy. Benefit from the ultrahigh NIR photothermal

[a]*School of Chemical and Material Engineering, Fuyang Normal University, Fuyang 236037, China. E-mail: hwang@fynu.edu.cn*

[b]*Institute of Industrial and Consumer Product Safety, Chinese Academy of Inspection and Quarantine, No. 11, Ronghua South Road, Beijing 100176, P. R. China. E-mail: xiguangcheng@caiq.org.cn*

† Electronic supplementary information (ESI) available. See DOI: 10.1039/c9ra09147e

conversion efficiency, the γ-Ti_3O_5 HPMs is also very attractive for technological uses on solar energy utilization, infrared light detection and so on.

2. Results and discussion

2.1. Electric structures of metallic γ-Ti_3O_5 and semiconducting TiO_2

As a titanium oxide with mixed valences, γ-Ti_3O_5 nanostructure is often used as vacuum optical coating material,[27–30] but it is rarely reported for other uses. Compared with semiconducting TiO_2, γ-Ti_3O_5 has many vastly different characteristics, such as high conductivity, high melting point, high chemical stability and so on.[31] The results of the first-principles calculation show that γ-Ti_3O_5 presents a metallic character rather than semiconducting properties. Fig. 1 shows the projected density of states (PDOS) of anatase TiO_2 (a titanium dioxide with the highest photocatalytic activity) and γ-Ti_3O_5. The PDOS of anatase TiO_2 distinctly presents the semiconductor character with a wide band gap, and the highest occupied states mainly composed from O 2p orbitals. Compared with TiO_2, the PDOS of γ-Ti_3O_5 shows an intrinsic metal character with the Fermi level crossing some bands, which benefits from the raise of Fermi level induced by oxygen defect, and most states of γ-Ti_3O_5 around the Fermi level are composed of Ti 3d orbitals. The calculation results suggest that the oxygen vacancy-rich γ-Ti_3O_5 contains large number of free d-orbital electrons, which makes it have the potential of photothermal conversion.

2.2. Structure and morphology characterizations

In order to obtain γ-Ti_3O_5 samples, we first prepared TiO_2 HPMs (Fig. S1†). Next, the TiO_2 HPMs were converted to γ-Ti_3O_5 HPMs by hydrogen reduction reaction. X-ray diffraction (XRD) pattern demonstrated that the as prepared products were completely indexed with the hexagonal γ-Ti_3O_5 with the cell parameters of $a = 9.970$ Å, $b = 5.074$ Å, and $c = 7.181$ Å (Fig. S2†). By calculating the half width of the (002) diffraction peak with Scherrer formula, the grain size of the γ-Ti_3O_5 powders is 215 nm, which is completely different from the white TiO_2 HPMs. The color of γ-Ti_3O_5 HPMs is black (Fig. 2a).

The morphology was characterized by scanning electron microscopy (SEM). As shown in Fig. 2b, the γ-Ti_3O_5 sample is composed of a large number of microspheres. The microsphere-size is about 3–10 μm. High-magnification SEM images reveal that these microspheres are actually assembled from a large number of ultrathin nanosheets, which thickness is only 2–3 nm (Fig. 2c and d). Fig. 2e shows a typical TEM image of one single HPM, which further reveals the hierarchical porous structure characteristics. Moreover, the TEM image also shows that the interior of these microspheres is hollow. The clear lattice fringes shown in the high resolution transmission electron microscopy (HRTEM) image reveals that the γ-Ti_3O_5 nanosheets are highly crystalline (Fig. 2f). The interplanar distance is about 0.337 nm, which can be refered to the (002) crystal face of γ-Ti_3O_5.

The chemical constituent of the γ-Ti_3O_5 HPMs are detected by energy-dispersive X-ray spectroscopy (EDS) analysis (Fig. S3†), which shows clear Ti and O signals. The O/Ti atomic ratio is about 1.68, which highly consistent with the theoretical atomic ratio of O/Ti in γ-Ti_3O_5 HPMs. The valence state of the ions in the γ-Ti_3O_5 HPMs is investigated using the X-ray photoelectron spectroscopy (XPS). As shown in Fig. S4,† the XPS characterizations reveal that the sample contains both Ti^{4+} and Ti^{3+} (Ti^{4+}/Ti^{3+} atomic ratio: 1/2). These trivalent titanium ions are the reason why the γ-Ti_3O_5 HPMs has metallic properties.

2.3. Localized-SPR effect and photothermal effect under simulited sunlight

Unlike TiO_2, which absorbs only ultraviolet light, the metallic γ-Ti_3O_5 HPMs show strong absorption throughout the visible region (400–700 nm), as shown in its ultraviolet-visible (UV-Vis) absorption spectroscopy (Fig. 3a). This strong absorption even extends to the near infrared (NIR, 700–1000 nm) region. It can be reasonably attributed to the local surface plasmon resonance (LSPR) of a large number of d-orbit free electrons contained in the γ-Ti_3O_5 HPMs.[39,40] In contrast, the TiO_2 HPMs had no significant absorption in the visible and NIR region.

A series of experiments displayed that these γ-Ti_3O_5 HPMs exhibited excellent photothermal conversion properties under xeon light (simulated sunlight) irradiation. As shown in Fig. 3b–

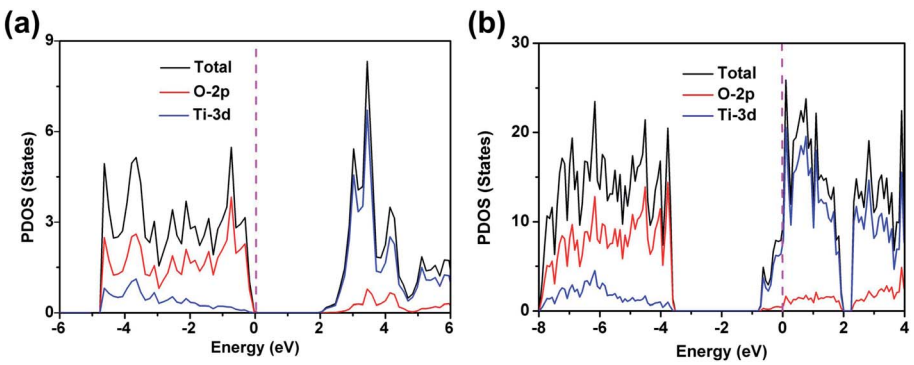

Fig. 1 The projected density of states of anatase TiO_2 (a) and γ-Ti_3O_5 (b), the magenta dash line is Fermi level.

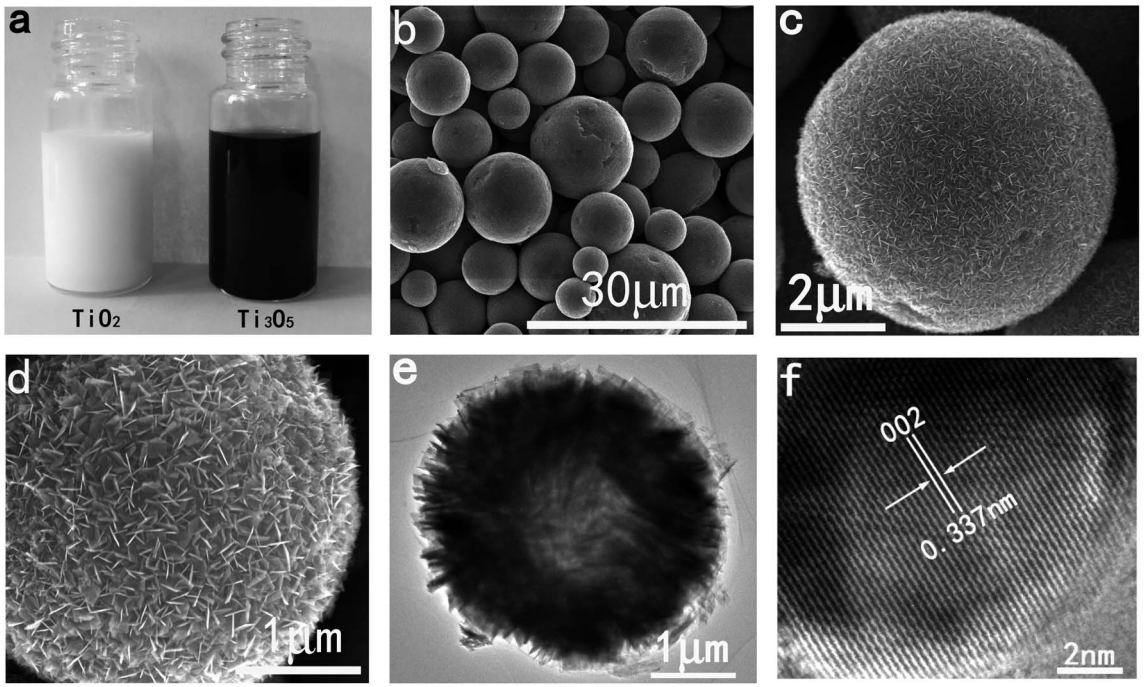

Fig. 2 Morphology and structure characterizations of the γ-Ti_3O_5 HPMs. (a) Color contrast between γ-Ti_3O_5 and TiO_2 HPMs. (b–d) SEM images of the γ-Ti_3O_5 HPMs. (e) TEM image of one single γ-Ti_3O_5 HPM. (f) HRTEM image of the γ-Ti_3O_5 nanosheets.

e, after irradiated by xeon light (2 kW m^{-2}) for 10 s, temperature of the γ-Ti_3O_5 HPMs quickly raised from room temperature to 96 °C. Under the same lighting conditions, the heating rate of γ-Ti_3O_5 is much higher than that of commercial graphene (Fig. 3f). For 0.01 g mL^{-1} aqueous suspension of γ-Ti_3O_5, the temperature can rise to 90 °C after sunlight irradiation (1 kW m^{-2}) for 10 minutes (Fig. 3g). Particularly interesting, when we put a sponge loaded with 0.3 g of γ-Ti_3O_5 HPMs on the surface of seawater, a lot of water vapor is produced after 5 min irradiation (2 kW m^{-2}), which indicates that the γ-Ti_3O_5 HPMs can be used as a promising seawater desalination material.

2.4. Photothermal property under NIR irradiation

Near infrared light is an ideal source for photothermal therapy due to its good biosecurity and deep tissue penetration.[41] As the γ-Ti_3O_5 HPMs showed strong absorption in the NIR region, their photothermal property was intensively investigated under NIR irradiation. Results revealed that the photothermal effect of γ-Ti_3O_5 HPMs under NIR laser irradiation was related with its concentration as well as the laser power density (Fig. 4). Fig. 4a showed the temperature evolution of γ-Ti_3O_5 HPMs at a series of concentrations under NIR laser irradiation with power density of 1 W cm^{-2} at 808 nm for 10 min. The temperature change (ΔT) of water was only 7.2 °C, while ΔT of 1 mg mL^{-1} of γ-Ti_3O_5 HPMs was up to 45.3 °C. ΔT decreased when the concentration of γ-Ti_3O_5 HPMs was reduced. In the first minutes of all concentration groups, the temperature increased rapidly. Then the increase smoothed gradually thereafter. Increase laser power could enhance the temperature rise (Fig. 4b). These results indicated that the treatment temperature could be controlled by adjusting the laser power and the concentration of γ-Ti_3O_5 during photothermal therapy.

To evaluate the photostability of γ-Ti_3O_5 HPMs, periodic laser on/off control with 808 nm laser were performed, in which the solution of 1 mg mL^{-1} γ-Ti_3O_5 HPMs was irradiated under 0.5 W cm^{-2} laser for 10 min, followed by naturally cooling down to the room temperature without laser irradiation. As shown in Fig. 4c, after 3 cycles of laser on/off irradiation, no notable decrease for the temperature elevation was observed during the experiment. The ΔT reached during the three photothermal cycles were 21.7 °C, 21.9 °C and 21.4 °C, respectively. Then, the γ-Ti_3O_5 HPMs suspension in water (1 mg mL^{-1}) was exposed to air for 28 days and their photothermal conversion properties were examined at predetermined time intervals (1, 7 and 28 days). As shown in Fig. 4d, for day 1, day 7 and day 28, the temperature increased by 21.7 °C, 21.5 °C and 18.1 °C respectively after 10 min of 0.5 W cm^{-2} laser irradiation. These results showed that γ-Ti_3O_5 HPMs had good repeated heating characteristics and photothermal stability.

The photothermal conversion efficiency of γ-Ti_3O_5 HPMs was calculated according to the method in former research.[31,33,42–44] The calculate detail was described in ESI.† The photothermal conversion efficiency (η) of γ-Ti_3O_5 HPMs irradiated by 808 nm laser can be calculated to be 65.29%. These results indicated the γ-Ti_3O_5 HPMs possess excellent NIR photothermal properties.

2.5. Stability of γ-Ti_3O_5 HPMs in physiological medium

The frequently used physiological medium, including phosphate-buffered saline (PBS, pH 7.4), cell culture medium

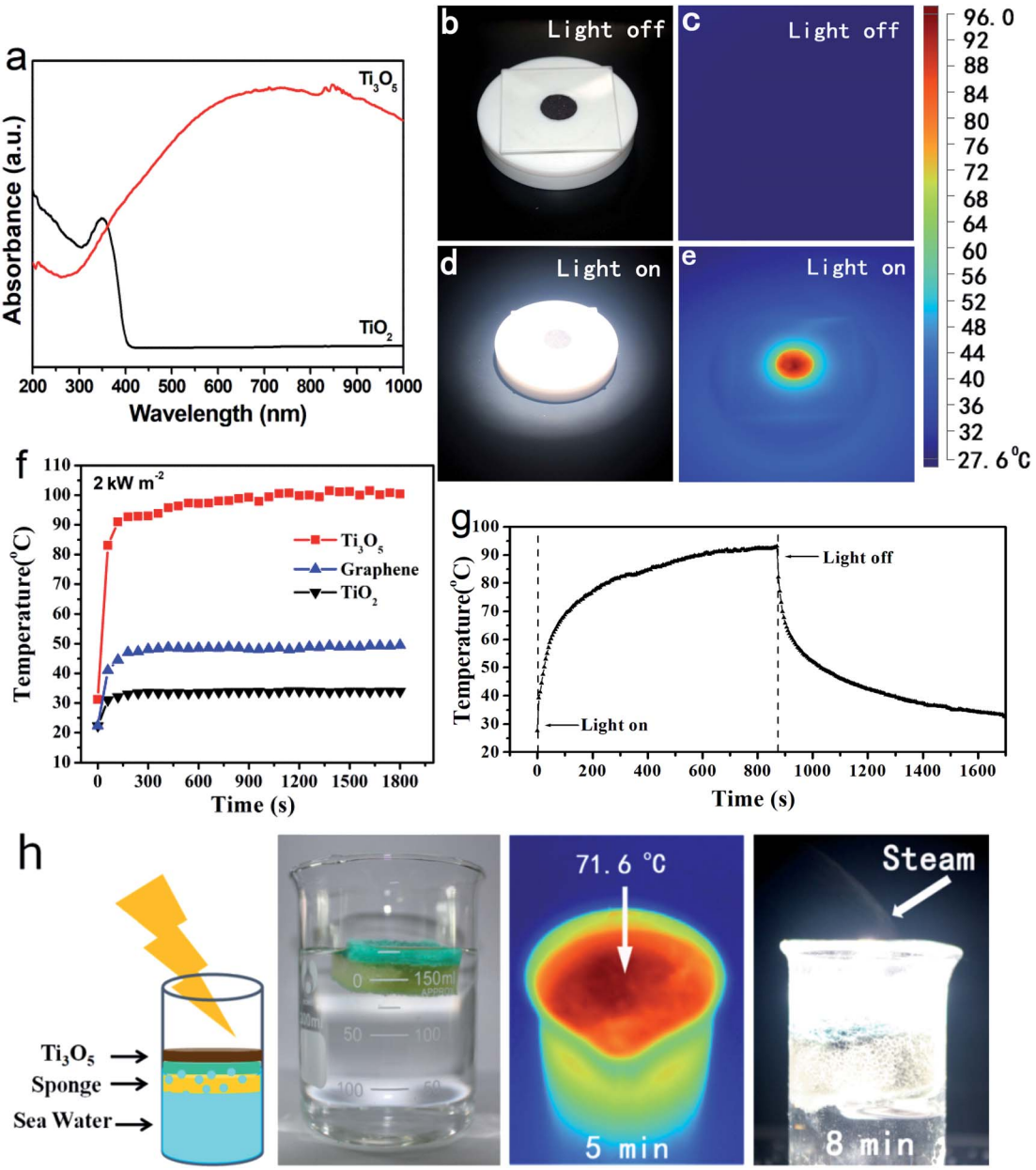

Fig. 3 Photothermal effect of the γ-Ti_3O_5 HPMs under simulated sunlight irradiation. (a) UV-Vis-NIR absorption of the γ-Ti_3O_5 HPMs. (b–e) Temperature-sensing IR photographs of the γ-Ti_3O_5 HPMs under the irradiation of simulated sunlight (2 kW m^{-2}). (f) Comparison of photothermal conversion properties of γ-Ti_3O_5 HPMs, graphene, and TiO_2 HPMs. (g) A typical time–temperature correlation curve of the γ-Ti_3O_5 suspension under simulated sunlight irradiation. (h) Simulated desalination process by using the γ-Ti_3O_5 HPMs as photothermal agent. In this experiment, the γ-Ti_3O_5 HPMs were loaded on a piece of cellulose sponge, and the irradiation power is 2 kW m^{-2}.

RPMI1640 and fetal bovine serum (FBS) were investigated to evaluated the stability of γ-Ti_3O_5 HPMs in physiological medium. As shown in Fig. S6 a,† γ-Ti_3O_5 HPMs precipitated after standing for 5 h. However, after precipitation at 5 h, the γ-Ti_3O_5 HPMs also can increase the temperature to 51.28/49.58 °C under 10 min irradiation by 808/980 nm laser (Fig. S6 b†). The suspension state could be easily recover after sonication. The absorption spectra displayed in Fig. S6 c† showed that the absorption feature did not change when the precipitation occurred in all kind of medium during 28 day observation, indicating that γ-Ti_3O_5 HPMs are highly stable in physiological medium.

2.6. *In vitro* photothermal therapy for cancer cells

The NIR photothermal therapy of γ-Ti_3O_5 HPMs for cancer cells was investigated by *in vitro* experiments using HeLa cells. As shown in Fig. 5a, without irradiation of NIR laser, no significant cytotoxicity could be observed in either TiO_2 or γ-Ti_3O_5 HPMs treated groups even at concentration up to 1 mg mL^{-1}. While, after irradiated with the 808 nm laser (2 W cm^{-2}) for 20 s (per

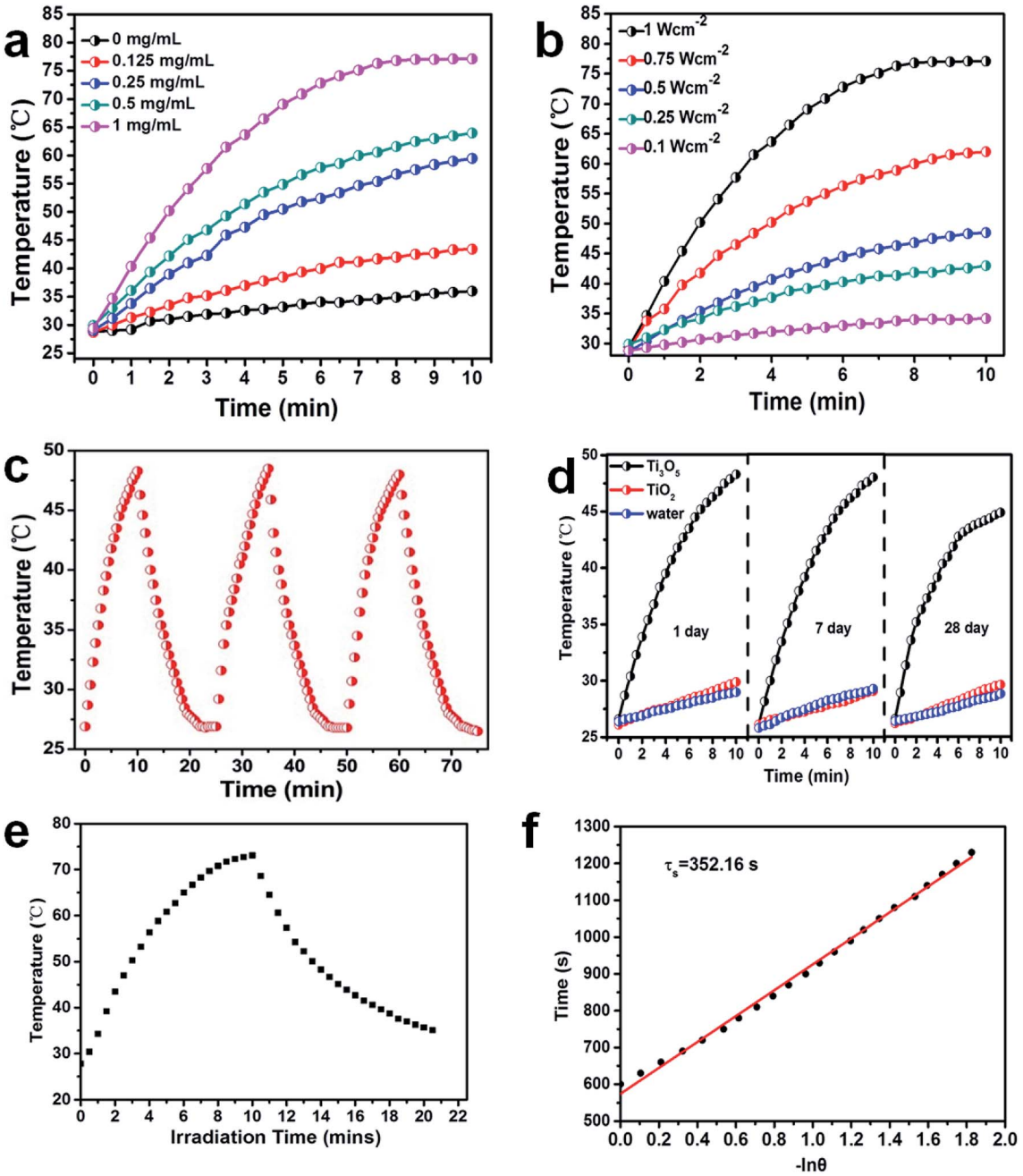

Fig. 4 Photothermal conversion efficiency of γ-Ti_3O_5 HPMs in aqueous dispersions under NIR-laser irradiation. (a) γ-Ti_3O_5 HPMs with different concentrations upon 808 nm laser irradiation (1 W cm^{-2}). (b) Different power of 808 nm laser irradiation at concentration of 1 mg mL^{-1} γ-Ti_3O_5 HPMs aqueous dispersion. (c) Temperature monitoring of γ-Ti_3O_5 HPMs solution at the concentration of 0.5 mg mL^{-1} during successive three cycles of an on-and-off 808 nm laser (1 W cm^{-2}). (d) Photothermal heating curves of 0.5 mg mL^{-1} γ-Ti_3O_5 and TiO_2 HPMs dispersed in water for 1 day, 7 days and 28 days and irradiated with the 808 nm laser (1 W cm^{-2}) for 10 min. (e) Photothermal effect of aqueous dispersion of γ-Ti_3O_5 (1 mg mL^{-1}) under irradiation with the NIR laser (808 nm, 1 W cm^{-2}) for one on/off cycle. (f) Time constant for heat transfer from the system is determined to be $\tau_s = 352.16$ s by applying the linear time data from the cooling period (after 600 s) *versus* negative natural logarithm of driving force temperature, which is obtained from the cooling stage of (e).

well), temperature in wells with γ-Ti_3O_5 HPMs increased up to 54.9 °C (Fig. S7†), and the cellular viability were significantly inhibited in a concentration related mode. On the contrary, direct irradiation of the cells in the absence of the γ-Ti_3O_5 HPMs or with TiO_2 HPMs did not inhibit the cell viability.

To confirm the results, cell apoptosis was observed by aridine orange/ethidium bromide (AO/EB) co-staining. In this method, nuclei in normal live cells were stained by AO with green fluorescence, the late apoptotic and dead cells were stained by EB with red fluorescence, and the early apoptotic cells were co-stained by both AO and EB showing orange

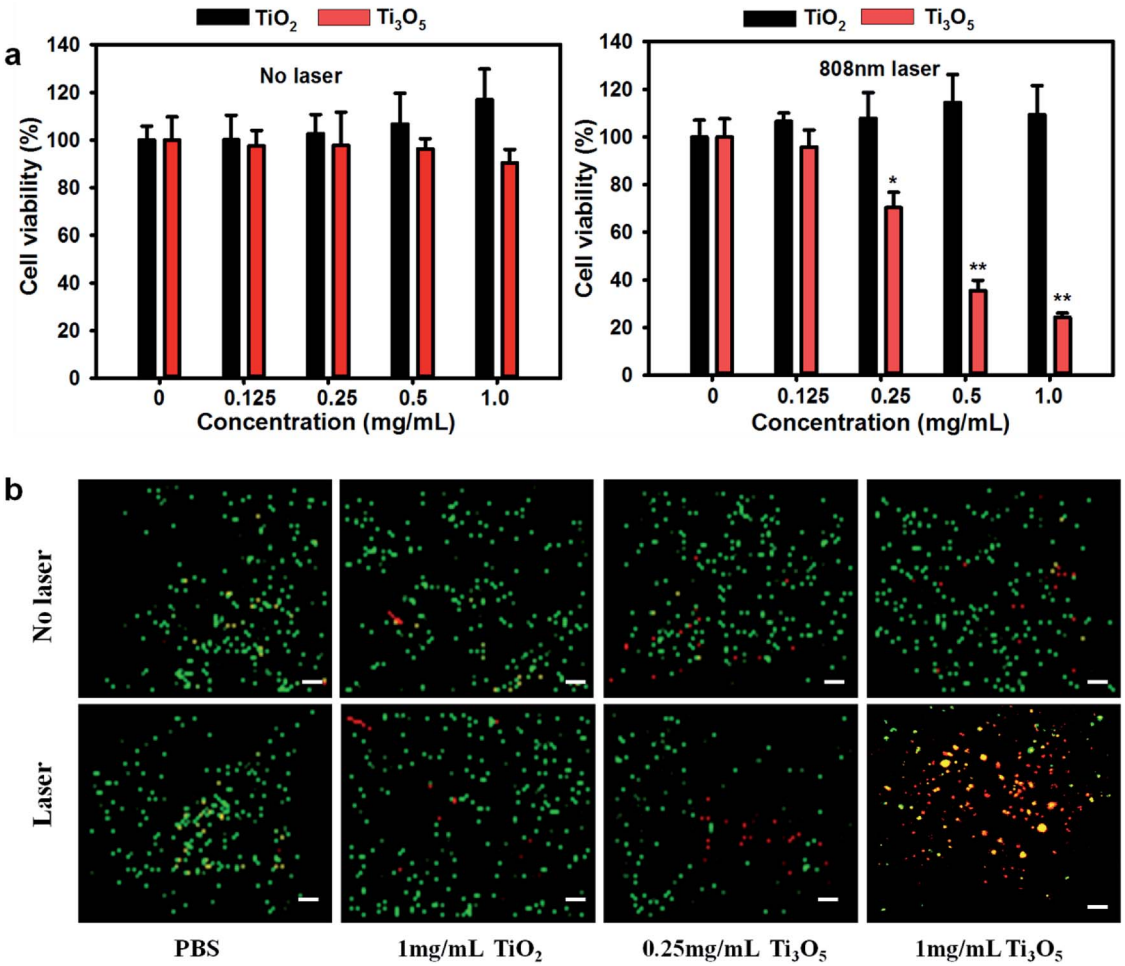

Fig. 5 (a) Relative viability of the HeLa cells after incubation with TiO_2 and γ-Ti_3O_5 HPMs (the concentration of nanoparticles was 0, 0.125, 0.25, 0.5 and 1 mg mL^{-1}) for 24 h with or without laser irradiation (2 W cm^{-2} for 30 s). (b) Fluorescence images of the HeLa cells after incubation with TiO_2 (1 mg mL^{-1}) and γ-Ti_3O_5 nanoparticles (0.25 mg mL^{-1} and 1 mg mL^{-1}) for 24 h and irradiation with the 808 nm laser (2 W cm^{-2}) for 30 s (live cells, green fluorescence; apoptotic cells, yellow fluorescence and dead cells, red fluorescence). *p < 0.05, **p < 0.01. Scale bar, 50 μm.

fluorescence.[33] As indicated in Fig. 5b, few dead cells could be found in both TiO_2 and γ-Ti_3O_5 HPMs exposure groups without laser irradiation. In PBS control groups, the laser irradiation did not induce significant cell damage. While, cell apoptosis and cell death were apparently increased in the γ-Ti_3O_5 HPMs exposure groups. These results indicated distinctive photothermal therapy for cancer cells *in vitro* by γ-Ti_3O_5 HPMs.

2.7. *In vivo* photothermal therapy for tumor tissues

The general toxicity *in vivo* of the γ-Ti_3O_5 HPMs was evaluated firstly. Results of haematological analysis indicated that there was no obvious changes for most of the haematological markers. The white blood cells, red blood cells, haemoglobin and haematocrit slight increase in the first day after γ-Ti_3O_5 treatment (Fig. S8†). At day 7 and day 28, these factors were recovered to normal level. The increase of white blood cell count on the first day may be the self-protective reaction of mice in order to exclude the foreign γ-Ti_3O_5 HPMs. The raise of red blood cells, haemoglobin and haematocrit could be induced by the interaction of γ-Ti_3O_5 and oxygen in blood. Ordinarily, the slight raise of red blood cells and related makers in short time does not affect the health.

The corresponding histological changes of organs (including liver, spleen, kidney, heart and lung) were investigated by immunohistochemistry using haematoxylin and eosin (H&E) staining (Fig. S9†). Compared with the control group, no histological abnormalities or lesions can be observed in TiO_2 or γ-Ti_3O_5 HPMs treated groups. In summary, γ-Ti_3O_5 HPMs exposed to the body of mice will not cause significant biological toxicity.

Photothermal therapy was performed for the treatment of tumor tissues by γ-Ti_3O_5 HPMs. *In vivo* cervical tumor model based on subcutaneous injection of HeLa cells was used in this work. According to the thermographic maps shown in Fig. 6a and b, the tumor surface temperatures of mice in γ-Ti_3O_5 HPMs treated groups increased from approximately 25.4 °C to 47 °C within 10 min of laser irradiation, which is high enough for tumor ablation.[12] Under the same conditions, the tumor surface temperature of the mice in both PBS and TiO_2 HPMs treated groups increased only 6.8 °C and 7.4 °C.

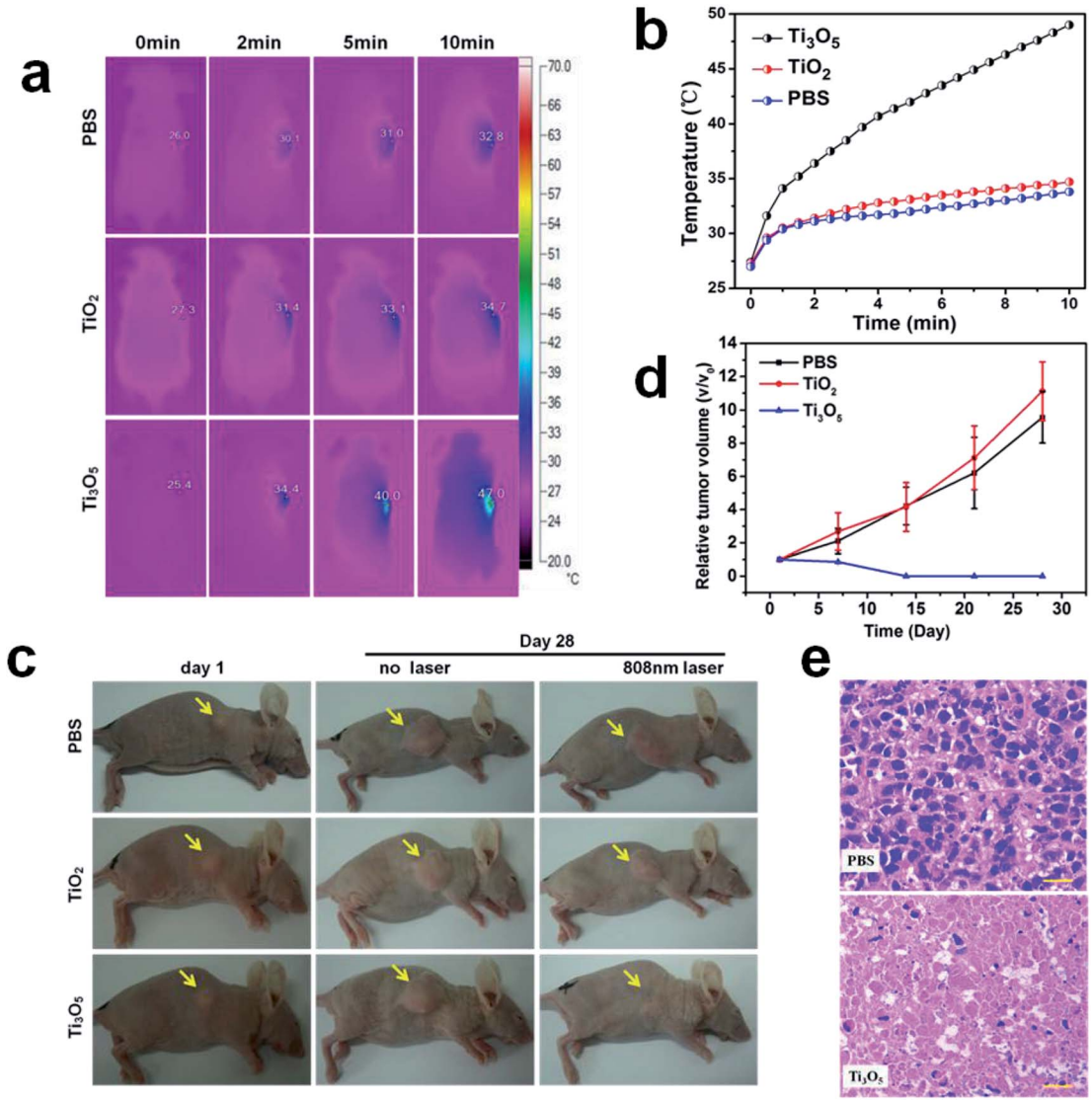

Fig. 6 *In vivo* photothermal therapy treatment using γ-Ti_3O_5 HPMs. (a) Infrared thermogram maps. (b) Photothermal heating curve of tumor-bearing nude mice received photothermal therapy. (c) Representative photographs of tumor growth at the 1st and 28th day in each group after PTT treatment. (d) Growth curves of tumor (volume changes) in different groups. (e) Histopathological observation of tumor slices (H&E staining) collected from PBS and γ-Ti_3O_5 treated groups after NIR irradiation. Scale bar, 20 μm.

The growth of tumor tissues was continually monitored every 7 days for 1 month after the initial laser irradiation. In contrast to the rapid tumor growth in control groups, tumors in mice treated with γ-Ti_3O_5 HPMs were completely eliminated 7 days after laser irradiation, and no reoccurrence was observed within 1 month (Fig. 6c and d). Similar with the results from the *in vitro* experiments, the TiO_2 HPMs showed no PTT effects to the tumor tissues.

The tumor tissues were collected for histopathological examination. As shown in Fig. 6e, γ-Ti_3O_5 HPMs with laser irradiation treatment induced obvious pyknosis, karyolysis and disappearance of nucleus in tumor tissues, indicating the γ-Ti_3O_5 HPMs were effective PTT agent for *in vivo* tumor ablation.

3. Conclusion

In summary, an interesting γ-Ti_3O_5 HPMs were prepared by a TiO_2-templated method. The aqueous dispersion of the γ-Ti_3O_5 HPMs exhibits obvious metallic feature and strong LSPR effect over the whole visible and NIR regions. As a photothermal agent, its PTT transfer conversion is calculated to be up to 65.29%. As a result, *in vitro* and *in vivo* experiments demonstrated that γ-Ti_3O_5 HPMs were biocompatible and could effectively inhibit growth of cancer cells and tumor tissues. Combined with their low cost, these findings reveal that the metallic γ-Ti_3O_5 HPMs are very promising in photothermal cancer therapy. Furthermore, considering its ultrahigh photothermal conversion efficiency, high biocompatibility and low

cost, this material has a very broad application prospects in the fields of solar energy utilization, NIR-light detection and so on.

4. Experimental section

4.1. Preparation of TiO_2 HPMs

In a typical synthesis, 30 mL of isopropanol (IPO) and 15 mL anhydrous ethanol (ET) were mixed into a solution, then 1 mL of tetrabutyl titanate (TBT) was slowly added into the solution and stirred for 1 h in air. The obtained mixture was transferred to a Teflon lined autoclave. Then the autoclave was heated at 160 °C for 8 h. After the reaction is completed, the autoclave is naturally cooled to room temperature, and the obtained white products were collected. The white powders were washed three times with ethanol and distilled water. Finally, the obtained brown powders were dried at 50 °C in air.

4.2. Synthesis of γ-Ti_3O_5 HPMs

In a typical synthesis, 1 g of the TiO_2 HPMs prepared above was put in an alumina crucible, which was placed in the middle part of a vacuum tube furnace (80 cm long and 5 cm in diameter). The tube furnace is heated to 500 °C and kept at this temperature for 2 hours. During heating, hydrogen is passed through the tube furnace with a rate of 30 mL min^{-1}. After the reaction was naturally cooled to room temperature, the obtained black products were collected.

4.3. Characterization of γ-Ti_3O_5 HPMs

The microstructure and morphology of the obtained γ-Ti_3O_5 HPMs were characterized by TEM (FEI Tecnai G2 F20 S-TWIN, USA) and SEM (Hitachi SU8010, Japan). The absorption spectrum of TiO_2 and γ-Ti_3O_5 HPMs in aqueous dispersions was examined with a UV-Vis-NIR spectroscope (Shimadzu UV-3600, Japan). The crystal structure of γ-Ti_3O_5 HPMs was investigated by XRD (Bruker D8, Germany). The average particle size of the γ-Ti_3O_5 HPMs (0.05 mg mL^{-1}) in the aqueous dispersion was measured using a Malvern laser particle size analyzer (Zetasizer Nano ZS90, UK).

4.4. Electronic structure calculations

All the first-principles calculations are based on density functional theory (DFT), are implemented through Vienna *Ab initio* Simulation Package (VASP). The local density approximation and an onsite Coulomb interaction (LDA+U) were used to calculate the periodic structure, where the *U–J* parameter was set to 4.2 eV for Ti 3d electrons. The cutoff energy was chosen at value of 500 eV and Brillouin zones (BZ) integrations were carried using Monkhorst–Pack sampling grids with the mesh density of $2\pi \times 0.2$ $Å^{-1}$ and $2\pi \times 0.1$ $Å^{-1}$ for structure optimizations and density of states calculations, respectively. The atomic positions and lattice constants were optimized using the conjugate gradients (CG) scheme until the force components on each atom were less than 0.02 eV $Å^{-1}$. And spin polarization was considered in all calculations.

4.5. Simulated sunlight induced heat conversion of γ-Ti_3O_5 HPM

0.3 g γ-Ti_3O_5 and TiO_2 HPMs were loaded in sample cells respectively and irradiated by xenon light (CeAulight Technology Co. Ltd. China) at 2 kW m^{-2} to investigate the photothermal properties. For simulated desalination experiment, γ-Ti_3O_5 HPMs were loaded on a piece of cellulose sponge floated in a beaker with 200 mL sea water. The temperature changes and images was recorded by the thermal imaging camera (Fluke Ti27, USA).

4.6. Laser induced heat conversion of γ-Ti_3O_5 HPMs

For laser irradiation experiment, the laser was generated by continuous semiconductor diode (Beijing Jing Xinda Biological Technology Co., Ltd. China). 1 mL of aqueous dispersions of γ-Ti_3O_5 HPMs at different concentrations in a quartz cuvette (side length, 1 cm) were irradiated by 1 W cm^{-2} 808 nm laser for 10 min. The real-time temperature is recorded by the thermal imaging camera (Fluke Ti27, USA). Photothermal curves of γ-Ti_3O_5 HPMs at concentration of 0, 0.125, 0.5 and 1.0 mg mL^{-1} were measured. In addition, the effect of laser power (0.1, 0.25, 0.5, 0.75, 1 W cm^{-2}) on the photothermal effect of γ-Ti_3O_5 HPMs (0.5 mg mL^{-1}) was also investigated.

To research the photothermal conversion stability of γ-Ti_3O_5 HPMs, periodic laser on/off control with 808 nm NIR light were used, in which the dispersions of γ-Ti_3O_5 HPMs was irradiated under NIR laser for 10 min, followed by naturally cooling down to the room temperature without NIR laser irradiation. Repeat the above process 3 times and record the temperature change curve. For long term stability of photothermal conversion of γ-Ti_3O_5 HPMs, the γ-Ti_3O_5 HPMs were dispersed in distilled water and kept in closed sample vials for 28 days. At time points of day 1, 7 and 28, the photothermal conversion stability was measured by the above method. TiO_2 HPMs were also investigated as comparison.

4.7. Stability of γ-Ti_3O_5 HPMs in physiological medium

To study the stability of γ-Ti_3O_5 HPMs in physiological medium, the 200 μg mL^{-1} γ-Ti_3O_5 HPMs suspension were prepared in ethanol, PBS buffer (pH 7.4), RPMI 1640 medium (supplemented with 10% fetal bovine serum) and fetal bovine serum (FBS). The as-prepared suspensions were sonicated for 15 min at 32 W. At the time point of 0, 1, 7 and 28 days, The UV-Vis-NIR absorption spectra was measured by UV-Vis-NIR spectrometer (UV-3600, Shimadzu, Japan).

4.8. *In Vitro* toxicity and photothermal experiments

Human cervixcarcinoma cell line (HeLa) was purchased from National Infrastructure of cell line Resource (Beijing, China). Cells were cultured in RPMI1640 medium supplemented with 10% fetal bovine serum (Gibco), 2 mM L-glutamine, 100 U mL^{-1} penicillin and 1 mg mL^{-1} streptomycin (Invitrogen) and incubated at 37 °C in an incubator with 5% CO_2.

In vitro toxicity and photothermal therapy were studied by methods previously reported in our former work.[33] For

cytotoxicity test, HeLa cells were seeded in 2 parallel 96-well plates (10^4 cells per well) and incubated overnight in the CO_2 incubator. Then the cells were treated with different concentrations of TiO_2 and γ-Ti_3O_5 HPMs (0, 0.125, 0.25, 0.5 and 1 mg mL^{-1}) for 12 h. Cells in one of the plates were rinsed with PBS and illuminated with the 808 nm laser (1 W cm^{-2}) for 20 s per well. Cells in another plate were not treated with laser. After irradiation, all cells were incubated for another 12 h. At the end of time point, the relative cell viabilities were determined by a standard MTT assay.[37]

For cellular apoptosis test, HeLa cells were seeded in 96-well plates (10^4 cells per well) and incubated overnight in the CO_2 incubator. After that, cells were treated with different concentrations of γ-Ti_3O_5 HPMs (0, 0.125, 0.25, 0.5 and 1 mg mL^{-1}) for 4 h and then illuminated with the 808 nm laser (1 W cm^{-2}) for 20 s per well. After irradiation, cells were incubated another 12 h and then rinsed with PBS, co-stained with acridine orange (AO) and ethidium bromide (EB) for 30 min. The stained cells were investigated by fluorescence microscope (DM6000B, Leica, Germany).

4.9. *In Vivo* toxicity and photothermal experiments

Experimental animals were purchased from the Beijing Vital River Laboratory Animal Technology Co., Ltd. (Beijing, China). All *in vivo* experiments were approved by the Animal Care and Use Committee of Chinese Academy of Inspection and Quarantine.

In vivo toxicity and photothermal therapy were studied by methods previously reported in our former work.[33] In brief, 45 healthy female Balb/c mice (6 weeks old) were randomly divided into 9 groups with 5 mice in each group: PBS control, TiO_2 and γ-Ti_3O_5 HPM groups for 3 time points (1, 7 and 28 days) respectively. About 100 μl of PBS, TiO_2 and γ-Ti_3O_5 HPMs were intravenously injected separately into the mice at the dose of 5 mg kg^{-1} mouse weight. At time points of day 1, 7 and 28 post injection, mice were narcotized and the peripheral blood was collected. 20 μL of whole blood was collected and analysed (MEK-7222K, Nihon Kohden Co., Ltd, Japan). The major organs (liver, spleen, kidney, heart and lung) were harvested and stained by H&E assay, then observed on microscopy (CTR 6000, Leica Microsystems Inc., Germany).

Tumor loaded female Balb/c nude mice (5 weeks old) were used for *in vivo* PTT therapy. The tumor model developed as the method in former works.[33,38] The mice were randomly divided into 3 groups (5 mice per group) and injected with 100 μL PBS, TiO_2 and γ-Ti_3O_5 HPMs (0.5 mg mL^{-1} in PBS) respectively into the tumor of the mice by intratumor injection. 1.5 h later, the entire region of the tumor was irradiated with the 808 nm NIR laser (1 W cm^{-2}) for 10 min. The temperature of the tumors and infrared thermographic maps were recorded by an infrared thermal imaging camera (Ti25, Fluke, USA) simultaneously.

The tumor sizes were measured every 7 days after irradiation using a caliper and calculated as the formula volume = (tumor length) × (tumor width)^2/2. It was regarded as '0' at its disappearance. The tumor measurements were performed by the same observer at all time points. Daily clinical observations were performed to monitor the animals for signs of distress. At the 28th day, all animals were euthanized. The tumor tissues were collected for histological analysis.

4.10. Statistical analysis

Data in this work were analysed by Origin Pro 9 and presented as means ± s.d. *T*-test was applied to test the significance of the observed differences between the study groups. A value of $p < 0.05$ was considered to be statistically significant.

Ethical statement

All animal procedures were performed in accordance with the Guidelines for Care and Use of Laboratory Animals of Institute of Industrial and Consumer Product Safety and approved by the Animal Ethics Committee of Chinese Academy of Inspection and Quarantine.

Conflicts of interest

There are no conflicts to declare.

Acknowledgements

This work received financial support from the Science Foundation of Chinese Academy of Inspection and Quarantine (2019JK004) and the National Key Research and Development Program of China (2017YFF0210003).

References

1 K. Yoshimatsu, O. Sakata and A. Ohtomo, *Sci. Rep.*, 2017, **7**, 12544.
2 J. Bogdan, J. Pławińska-Czarnak and J. Zarzyńska, *Nanoscale Res. Lett.*, 2017, **12**, 225.
3 S. Ohkoshi, Y. Tsunobuchi, T. Matsuda, K. Hashimoto, A. Namai, F. Hakoe and H. Tokoro, *Nat. Chem.*, 2010, **2**, 539.
4 H. Tokoro, M. Yoshikiyo, K. Imoto, A. Namai, T. Nasu, K. Nakagawa, N. Ozaki, F. Hakoe, K. Tanaka, K. Chiba, R. Makiura, K. Prassides and S. Ohkoshi, *Nat. Commun.*, 2015, **6**, 7037.
5 X. Chen, Y. Chen, M. Yan and M. Qiu, *ACS Nano*, 2012, **6**, 2550.
6 Q. Tian, M. Tang, Y. Sun, R. Zou, Z. Chen, M. Zhu, S. Yang, J. Wang, J. Wang and J. Q. Hu, *Adv. Mater.*, 2011, **23**, 3542.
7 J. Shao, H. Xie, H. Huang, Z. Li, Z. Sun, Y. Xu, Q. Xiao, X. Yu, Y. Zhao, H. Zhang, H. Wang and P. K. Chu, *Nat. Commun.*, 2016, **7**, 12967.
8 S. Kang, S. H. Bhang, S. Hwang, J. K. Yoon, J. Song, H. K. Jang, S. Kim and B. S. Kim, *ACS Nano*, 2015, **9**, 9678.
9 D. B. B. Van, N. Devoogdt, A. D'hollander, H. L. Gijs, K. Jans, L. Lagae, S. Muyldermans, G. Maes and G. Borghs, *ACS Nano*, 2011, **5**, 4319.
10 P. Wang, L. Zhang, W. Zheng, L. Cong, Z. Guo, Y. Xie, L. Wang, R. Tang, Q. Feng, Y. Hamada, K. Gonda, Z. Hu, X. Wu and X. Jiang, *Angew. Chem., Int. Ed.*, 2018, **130**, 1491.

11 A. K. Rengan, A. B. Bukhari, A. Pradhan, R. Malhotra, R. Banerjee, R. Srivastava and A. De, *Nano Lett.*, 2015, **15**, 842.
12 Z. Li, H. Huang, S. Tang, Y. Li, X. F. Yu, H. Wang, P. Li, Z. Sun, H. Zhang, C. Liu and P. K. Chu, *Biomaterials*, 2016, **74**, 144.
13 Q. Dong, X. Wang, X. Hu, L. Xiao, L. Zhang, L. Song, M. Xu, Y. Zou, L. Chen, Z. Chen and W. Tan, *Angew. Chem., Int. Ed.*, 2018, **57**, 177.
14 W. Xue, J. Zhou, D. Gao, F. Gao, Z. Wang, L. Luo, Y. Lia and Z. Liua, *New J. Chem.*, 2015, **39**, 3608.
15 J. G. Piao, F. Gao, Y. Li, L. Yu, D. Liu, Z. B. Tan, Y. Xiong, L. Yang and Y. Z. You, *Nano Res.*, 2018, **11**, 3193.
16 J. Chen, D. Wang, J. Xi, L. Au, A. Siekkinen, A. Warsen, Z. Y. Li, H. Zhang, Y. Xia and X. Li, *Nano Lett.*, 2007, **7**, 1318.
17 J. W. Xiao, S. X. Fan, F. Wang, L. D. Sun, X. Y. Zheng and C. H. Yan, *Nanoscale*, 2014, **6**, 4345.
18 S. Shi, X. Chen, J. Wei, Y. Huang, J. Weng and N. Zheng, *Nanoscale*, 2016, **8**, 5706.
19 H. K. Moon, H. L. Sang and H. C. Choi, *ACS Nano*, 2009, **3**, 3707.
20 L. M. Maestro, P. Haro-González, R. B. Del, J. Ramiro, A. J. Caamaño, E. Carrasco, A. Juarranz, F. S. Rodríguez, J. G. Sole and D. Jaque, *Nanoscale*, 2013, **5**, 7882.
21 B. P. Jiang, L. F. Hu, X. C. Shen, S. C. Ji, Z. Shi, C. J. Liu, L. Zhang and H. Liang, *ACS Appl. Mater. Interfaces*, 2014, **6**, 18008.
22 M. Sinha, G. Gollavelli and Y. C. Ling, *RSC Adv.*, 2016, **6**, 63859.
23 Y. Liu, K. Ai, J. Liu, M. Deng, Y. He and L. Lu, *Adv. Mater.*, 2013, **25**, 1353.
24 Y. Cao, J. H. Dou, N. J. Zhao, S. Zhang, Y. Q. Zheng, J. P. Zhang, J. Y. Wang, J. Pei and Y. Wang, *Chem. Mater.*, 2016, **29**, 718.
25 Y. Yang, W. Zhu, Z. Dong, Y. Chao, L. Xu, M. Chen and Z. Liu, *Adv. Mater.*, 2017, **29**, 1703588.
26 Z. Zha, X. Yue, Q. Ren and Z. Dai, *Adv. Mater.*, 2013, **25**, 777.
27 S. Cong, Y. Yuan, Z. Chen, J. Hou, M. Yang, Y. Su, Y. Zhang, L. Li, Q. Li, F. Geng and Z. Zhao, *Nat. Commun.*, 2015, **6**, 7800.
28 G. Xi, S. Ouyang, P. Li, J. Ye, Q. Ma, N. Su, H. Bai and C. Wang, *Angew. Chem., Int. Ed.*, 2012, **51**, 2395.
29 G. Xi, J. Ye, Q. Ma, N. Su, H. Bai and C. Wang, *J. Am. Chem. Soc.*, 2012, **134**, 6508.
30 D. Ding, W. Guo, C. Guo, J. Sun, N. Zheng, F. Wang, M. Yana and S. Liu, *Nanoscale*, 2017, **9**, 2020.
31 L. Yuwen, J. Zhou, Y. Zhang, Q. Zhang, J. Shan, Z. Luo, L. Weng, Z. Teng and L. Wang, *Nanoscale*, 2016, **8**, 2720.
32 J. Du, X. Zheng, Y. Yong, J. Yu, X. Dong, C. Zhang, R. Zhou, B. Li, L. Yan, C. Chen, Z. Gu and Y. Zhao, *Nanoscale*, 2017, **9**, 8229.
33 W. Liu, X. Li, W. Li, Q. Zhang, H. Bai, J. Li and G. Xi, *Biomaterials*, 2018, **163**, 43.
34 P. Thevenot, J. Cho, D. Wavhal, R. B. Timmons and L. Tang, *Nanomed. Nanotechnol. Biol. Med.*, 2008, **4**, 226.
35 Z. Youssef, R. Vanderesse, L. Colombeau, F. Baros, T. Roques-Carmes, C. Frochot, H. Wahab, J. Toufaily, T. Hamieh, S. Acherar and A. M. Gazzali, *Cancer Nanotechnol.*, 2017, **8**, 6.
36 R. C. Gilson, K. C. L. Black, D. D. Lane and S. Achilefu, *Angew. Chem., Int. Ed.*, 2017, **129**, 10717.
37 T. Mosmann, *J. Immunol. Methods*, 1983, **65**, 55.
38 Z. Xiao, C. Ji, J. Shi, E. M. Pridgen, J. Frieder, J. Wu and O. C. Farokhzad, *Angew. Chem., Int. Ed.*, 2012, **124**, 12023.
39 K. Manthiram and A. P. Alivisatos, *J. Am. Chem. Soc.*, 2012, **134**, 3995.
40 T. R. Gordon, M. Cargnello, T. Paik, F. Mangolini, R. T. Weber, P. Fornasiero and C. B. Murray, *J. Am. Chem. Soc.*, 2012, **134**, 6751.
41 M. Chu, Y. Shao, J. Peng, X. Dai, H. Li, Q. Wu and D. Shi, *Biomaterials*, 2013, **34**, 4078.
42 K. Dou, W. Zhu, Y. Zou, Y. Gu, J. Li, S. Zhang, Z. Liu and H. Zeng, *J. Mater. Chem. B*, 2017, **5**, 7393.
43 D. K. Roper, W. Ahn and M. Hoepfner, *J. Phys. Chem. C*, 2007, **111**, 3636.
44 Q. Tian, F. Jiang, R. Zou, Q. Liu, Z. Chen, M. Zhu, S. Yang, J. Wang, J. Wang and J. Hu, *ACS Nano*, 2011, **5**, 9761.

